This is a peer-reviewed, author's accepted manuscript of the following research article:
Luo, J., Shao, H., Cao, H., Chen, X., Cai, B., & Liu, B. (2022).
Modified DSAN for unsupervised cross-domain fault diagnosis of bearing under speed fluctuation.
Journal of Manufacturing Systems, 180-191. https://doi.org/10.1016/j.jmsy.2022.09.004

Modified DSAN for unsupervised cross-domain fault diagnosis of bearing under speed fluctuation

Jingjie Luo[1], Haidong Shao[1, 2*], Hongru Cao[1], Xingkai Chen[1], Baoping Cai[3], Bin Liu[4]

1 College of Mechanical and Vehicle Engineering, Hunan University, Changsha 410082, China

2 Department of Civil, Environmental and Natural Resources Engineering, Luleå University of Technology, Luleå 97187, Sweden

3 College of Mechanical and Electronic Engineering, China University of Petroleum, Qingdao 266580 China

4 Department of Management Science, University of Strathclyde, Glasgow G1 1XQ, UK

Corresponding author: Haidong Shao (hdshao@hnu.edu.cn)

Abstract: Existing researches about unsupervised cross-domain bearing fault diagnosis mostly consider global alignment of feature distributions in various domains, and focus on relatively ideal diagnosis scenario under the steady speeds. Therefore, unsupervised feature adaptation between all the corresponding subdomains under speed fluctuation remains great challenges. This paper proposes a modified deep subdomain adaptation network (MDSAN) for more practical and challenging cross-domain diagnostic scenarios from the fluctuating speeds to steady speeds. Firstly, to extract the representative features and effectively suppress negative transfer, a novel shared feature extraction module guided by multi-headed self-attention mechanism is constructed. Then, a new trade-off factor is designed to improve the convergence performance and optimization process of MDSAN. The proposed method is used for analyzing experimental bearing vibration data, and the results show that it has higher diagnostic accuracy, faster convergence, better distribution alignment, and is more suitable for unsupervised cross-domain fault diagnosis under speed fluctuation scenario compared with the existing methods.

Keywords: modified deep subdomain adaptation network; cross-domain bearing fault diagnosis; speed fluctuation; multi-headed self-attention mechanism; new trade-off factor

1. Introduction

Health status of bearings directly affects the stable and reliable operation of rotating machinery. It is of vital significance to determine their status using intelligent diagnostic methods [1-4]. In recent years, because of its excellent feature extraction and learning capability, deep learning has been widely adopted to intelligent fault diagnosis of bearings and other mechanical components [5-11]. However, these intelligent diagnosis studies based on deep learning assume that the training and test samples should be independently and identically distributed, and the training samples should contain abundant label information. In practical tasks, it is difficult to ensure that the collected data samples have the same distribution characteristics due to the change of rotational speed, working load, and other factors.

In addition, the cost of obtaining large number of labeled samples under various fault modes is high. Therefore, it is more practical to investigate cross-domain unsupervised fault diagnosis [12-18].

Unsupervised domain adaptation aims to narrow the gap between the labeled source-domain samples and unlabeled target-domain samples through feature transformation [19-21]. In the past several years, unsupervised domain adaptation has gained an increasing attention in cross-domain mechanical fault diagnosis. In 2018, Li *et al.* [22] used a domain adaptation network built on multi kernels maximum mean discrepancy (MK-MMD) to improve the robustness for bearing fault diagnosis against noise and variable operating conditions. In 2019, Han *et al.* [23] adopted domain adversarial neural network (DANN) to learn domain invariant features and avoid overfitting for fault detection. The approach was applied for fault diagnosis of a wind turbine under different wind speeds and a generic gearbox under different rotational speeds, respectively. In 2020, a multi-task learning model with joint maximum mean discrepancy (JMMD) was utilized by Chen *et al.* [24] to narrow differences of marginal and conditional distribution for diagnostic scenarios of different planetary gearbox under two sun gear rotation frequencies and two loads. In 2020, to achieve classification of bearings and gears under various rotating speeds, Li *et al.* [25] constructed new domain adversarial transfer network, handling remarkable distribution discrepancy across rotating speeds. In 2021, Qin *et al.* [26] added the CORAL loss into parameter sharing adversarial domain adaptation networks to promote domain confusion when state identification was required for one-stage planetary gearboxes under different speed conditions. In 2022, an interactive dual adversarial network was designed by Mao *et al.* [27], which could distinguish the unseen states precisely and report the known health states concurrently of rolling bearing and the planetary gearbox under different loads and speeds, respectively. In 2022, in presence of imbalanced bearing fault diagnosis for rolling bearings under different speeds, Wu *et al.* [28] developed a cost-sensitive domain adaptation network, aiming at solving the domain variance and class imbalance problems.

However, challenges still exist in spite of the above researches, detailed as follows. (1) The above studies are all based on the global alignment strategy, while ignoring the respective alignment of each individual subdomain, which may influence local alignment of source and target domains and classification performance [29]. (2) The feature extraction modules constructed in the above studies fail to evaluate and select the representative features of each class according to their importance, which may degrade suppression of negative transfer. As a result, the knowledge learned on the source domain may have a negative effect on learning of the target domain [30]. (3) All of the above studies focus on the relatively ideal fault diagnosis scenario under the steady rotational speed. However, speed fluctuations will inevitably occur during practical production process, in which the acquired original signals represent strong non-stationary characteristics and include interference [31]. Thus, unsupervised cross-domain feature adaptation and fault diagnosis under speed fluctuation is a meaningful yet challenging study, which demands more advanced techniques.

In this article, a novel approach using modified deep subdomain adaptation network (MDSAN) is put forward for unsupervised cross-domain bearing fault diagnosis under speed fluctuation. A series of

experimental datasets of bearing and comparative tests are used for demonstrating the feasibility and superiority of the proposed approach. Our contributions are described as follows.

(1) In order to extract the representative features hidden in the complex signals corresponding to each fault mode and effectively suppress negative transfer, a novel shared feature extraction module guided by multi-headed self-attention mechanism is constructed.

(2) A new trade-off factor is designed to improve the convergence performance and optimization process.

(3) A new method based on MDSAN is proposed for more practical and challenging cross-domain diagnostic scenarios from the fluctuating speeds to steady speeds, through aligning the local distribution of corresponding subdomains.

The framework of this article can be organized as follows. Section 2 introduces the concepts related to subdomain adaptation. Section 3 describes the proposed approach in this paper. In Section 4, validation cases are then performed with unsupervised cross-domain bearing fault diagnosis under speed fluctuation. At last, conclusions and follow-up research are given in Section 5.

2. Unsupervised subdomain adaptation

Fig. 1 shows that subdomain adaption exploits the distribution relationship between two subdomains belonging to source and target domains respectively. It avoids mere global alignment, which leads to the reduction of the distances between samples of different classes, accompanied by inaccurate classification.

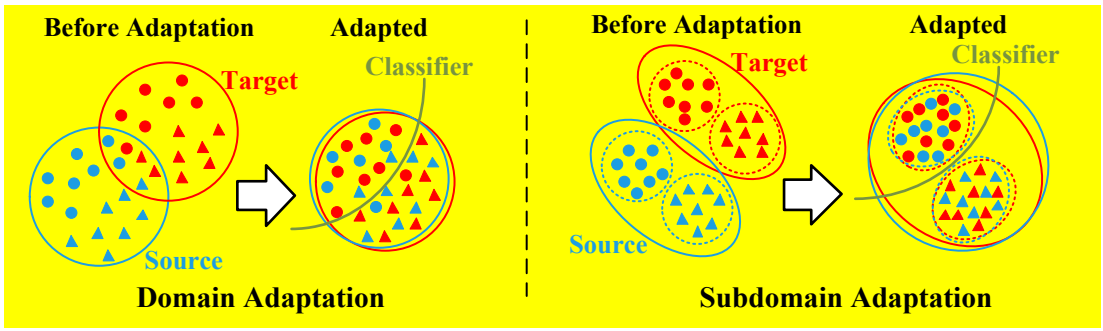

Fig. 1. Domain adaptation and subdomain adaptation

Relevant definitions of unsupervised subdomain adaptation are given as follows [32-34]. Let $\mathcal{D}_s = \{(\mathbf{x}_i^s, \mathbf{y}_i^s)\}_{i=1}^{n_s}$ be the source domain, in which $\mathbf{x}_i^s$ is the ith source-domain labeled sample with the label of $\mathbf{y}_i^s$, and n_s is the number of source-domain samples. Let $\mathcal{D}_t = \{\mathbf{x}_j^t\}_{j=1}^{n_t}$ be the target domain, in which $\mathbf{x}_j^t$ represents the jth target-domain unlabeled sample with the pseudo label of $\hat{\mathbf{y}}_j^t$, and n_t represents the number of target-domain samples. All samples belonging to the same class in each domain are assumed to be a subdomain. Let C denote the number of classes, and then $\mathcal{D}_s$ and $\mathcal{D}_t$ are both divided into C subdomains: $\mathcal{D}_s^{(c)}$ and $\mathcal{D}_t^{(c)}$, respectively, where c indicates the class label ($c \in \{1, 2, \cdots, C\}$).

The goal of unsupervised subdomain adaptation is to train a deep network $\mathbf{y} = f(\mathbf{x})$ which can

capture transferable features and then align distributions of related subdomains. Thus, the total loss function of unsupervised subdomain adaptation is

$$\min_{f} \frac{1}{n_s}\sum_{i=1}^{n_s} J(f(\mathbf{x}_i^s),\mathbf{y}_i^s)+\lambda \mathbf{E}_c[\hat{d}(p^{(c)},q^{(c)}) \tag{1}$$

in which $J(.,.)$ refers to the cross-entropy loss, $\mathbf{E}_c[.]$ is mathematical expectation, $\hat{d}(.,.)$ is the subdomain adaptation loss, $p^{(c)}$ and $q^{(c)}$ refer to distributions of $\mathcal{D}_s^{(c)}$ and $\mathcal{D}_t^{(c)}$, respectively, and λ is used as a positive trade-off factor between the above two loss functions.

3. The proposed method

3.1. Design of novel shared feature extraction module

For signals under speed fluctuation, in order to extract the representative features hidden in the complex signals corresponding to each fault mode and effectively suppress negative transfer, this paper constructs a novel shared feature extraction module guided by multi-headed self-attention mechanism.

The attention mechanism can highlight faulty features with important information and suppress invalid features [35-37]. Self-attention mechanism is an improvement of the attention mechanism, which pays more attention to the internal correlation of sample data. Its structure can be found in **Fig 2** and the mathematical expressions are

$$\begin{cases} \mathbf{Q}=\mathbf{W}^q\mathbf{I} \\ \mathbf{K}=\mathbf{W}^k\mathbf{I} \\ \mathbf{V}=\mathbf{W}^v\mathbf{I} \\ \boldsymbol{Attention}(\mathbf{Q},\mathbf{K},\mathbf{V})=\boldsymbol{Softmax}\left(\dfrac{\mathbf{Q}\mathbf{K}^T}{\sqrt{d_k}}\right)\mathbf{V} \end{cases} \tag{2}$$

in which $\mathbf{I}$ denotes a time-series vector representing input vibration data, $\mathbf{W}^q$, $\mathbf{W}^k$, and $\mathbf{W}^v$ are the three different weight matrices required for the linear mapping of $\mathbf{I}$, respectively, $\mathbf{Q}$ and $\mathbf{K}$ are the information mapping of the data at the current moment and at other times, respectively, $\mathbf{V}$ denotes the feature mapping of the input vector itself, the dot product of $\mathbf{Q}$ and $\mathbf{K}$ can be used to characterize the correlation between data, d_k refers to the dimension of the input vector, ***Softmax*** is the normalization function, and ***Attention*** denotes the final calculated result.

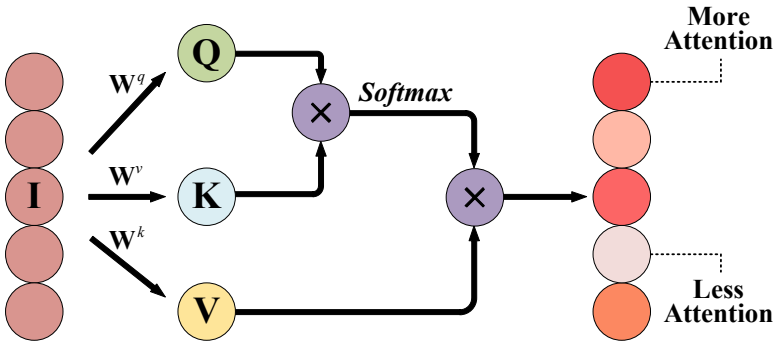

Fig. 2. Principle diagram of self-attention mechanism

In order to capture richer features and information, multiple **Q**, **K**, **V** are used for each data for information and feature mapping, which is called multi-headed self-attention mechanism (MHSAM). MHSAM establishes a content view of global relationships for bearing fault signals under speed fluctuation from multiple perspectives, allowing selective aggregation of global features. Its mathematical expression is provided as follows.

$$\begin{cases} \boldsymbol{head}_i = \boldsymbol{Attention}(\mathbf{Q}\mathbf{W}_i^q, \mathbf{K}\mathbf{W}_i^k, \mathbf{V}\mathbf{W}_i^v) \\ \boldsymbol{MultiHead}(\mathbf{Q},\mathbf{K},\mathbf{V}) = \boldsymbol{Concat}(\boldsymbol{head}_1, \cdots, \boldsymbol{head}_n) \end{cases} \tag{3}$$

where each $\boldsymbol{head}_i$ will compute the respective self-attention score, and the information learned from different heads is combined by ***Concat***.

Fig. 3 shows the framework details of the designed novel shared feature extraction module, including one input layer, four 1D convolutional layers (Conv), two 1D max pooling layers, one MHSAM layer, and a fully connected layer (FC). Each Conv is followed by a 1D batch normalization (BN) [38] and a ReLU activation function. Furthermore, the second ReLU is connected to a max pooling layer. The fourth ReLU is linked to a adaptive max pooling layer to achieve input length adaptation. It is then followed by a MHSAM layer to excavate deeply into the timing relationships inherent in bearing vibration signals under speed fluctuation. The output is thereafter flattened and passed through a FC, a ReLU and a dropout layer. Both the source and target domains use this feature extraction module. **Table 1** shows the specific parameters.

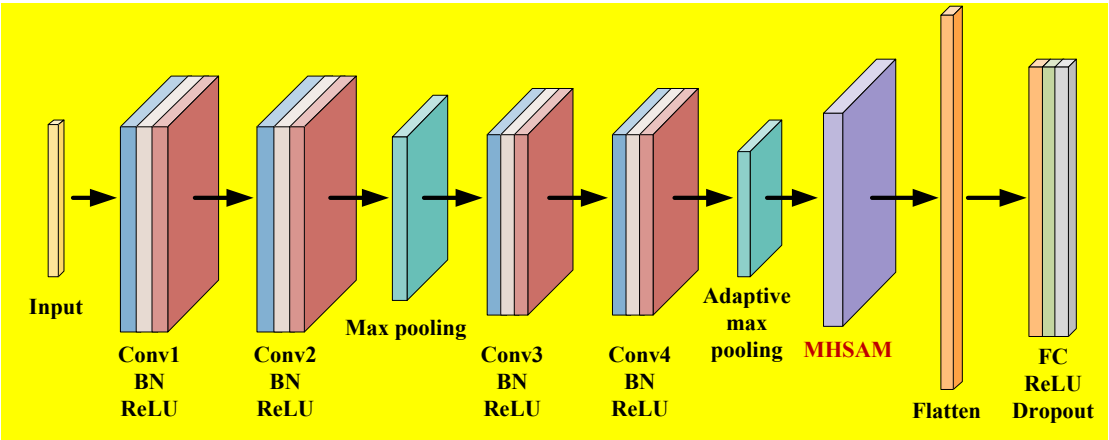

Fig. 3. Structure of the novel shared feature extraction module

Table 1
Parameters of the novel shared feature extraction module

Layers	Parameters
Conv1	Out channels=16, Kernel size=15
Conv2	Out channels=32, Kernel size=3
Max pooling	Kernel size=2, Stride=2
Conv3	Out channels=64, Kernel size=3
Conv4	Out channels=128, Kernel size=3
Adaptive max pooling	Output size=4

MHSAM	Hidden size = 128, Heads = 8
FC	Out features=256
Dropout	0.5

3.2. Construction and training of MDSAN

In order to align the relevant subdomains, local maximum mean discrepancy (LMMD) [29] is adopted to measure the difference between two subdomains, defined as follows.

$$d_{\mathcal{H}}(p,q) \triangleq \mathbf{E}_c \left\| \mathbf{E}_{p^{(c)}}[\phi(\mathbf{x}^s)] - \mathbf{E}_{q^{(c)}}[\phi(\mathbf{x}^t)] \right\|_{\mathcal{H}}^2 \tag{4}$$

in which $\mathbf{x}^s$ and $\mathbf{x}^t$ denote instances of $\mathcal{D}_s$ and $\mathcal{D}_t$, respectively, $\mathcal{H}$ represents the reproducing kernel Hilbert space assigned with a characteristic kernel k, and $\phi(.)$ denotes a mapping from the initial space to the Hilbert space [39]. Through minimizing **Eq. (4)**, the distributions of subdomains belonging to the same class are then closer.

The weights w^c are assigned to the samples of each class. Thus, the LMMD can then be acquired by

$$\hat{d}_{\mathcal{H}}(p,q) = \frac{1}{C}\sum_{c=1}^{C} \left\| \sum_{\mathbf{x}_i^s \in \mathcal{D}_s} w_i^{sc}\phi(\mathbf{x}_i^s) - \sum_{\mathbf{x}_j^t \in \mathcal{D}_t} w_j^{tc}\phi(\mathbf{x}_j^t) \right\|_{\mathcal{H}}^2 \tag{5}$$

where w_i^{sc} and w_j^{tc} indicate the weights of $\mathbf{x}_i^s$ and $\mathbf{x}_j^t$ belonging to class c, respectively, and $\sum_{\mathbf{x}_i \in \mathcal{D}} w_i^c \phi(\mathbf{x}_i)$ is the weighted sum of class c. For the specific calculation of w_i^{sc} and w_j^{tc}, one can refer to [29].

Let $\mathbf{z}^s$ and $\mathbf{z}^t$ denote the output features of the samples from two different domains after passing through the novel shared feature extraction module, respectively. Then the following expression can be directly used as the LMMD:

$$\begin{aligned} \hat{d}_{\mathcal{H}}(p,q) = \frac{1}{C}\sum_{c=1}^{C} \Bigg[& \sum_{i=1}^{n_s}\sum_{j=1}^{n_s} w_i^{sc} w_j^{sc} k(\mathbf{z}_i^s, \mathbf{z}_j^s) \\ & + \sum_{i=1}^{n_t}\sum_{j=1}^{n_t} w_i^{tc} w_j^{tc} k(\mathbf{z}_i^t, \mathbf{z}_j^t) - 2\sum_{i=1}^{n_s}\sum_{j=1}^{n_t} w_i^{sc} w_j^{tc} k(\mathbf{z}_i^s, \mathbf{z}_j^t) \Bigg] \end{aligned} \tag{6}$$

in which $k(\mathbf{z}_i^s, \mathbf{z}_j^t)$ is the kernel function using linear combinations of multiple Gaussian kernels [40].

MDSAN uses the LMMD of **Eq. (7)** as the subdomain adaptation loss function. Then the overall training objective function are calculated similarly to **Eq. (1)** as follows.

$$\min_f \frac{1}{n_s}\sum_{i=1}^{n_s} J(f(\mathbf{x}_i^s), \mathbf{y}_i^s) + \lambda \hat{d}_{\mathcal{H}}(p,q) \tag{7}$$

in which the former is the cross-entropy classification loss, the latter is LMMD loss, and λ is a trade-off factor of the two terms.

Throughout the training process, standard mini-batch stochastic gradient descent (mini-batch SGD)

algorithm is employed to compute MDSAN. In the existing DSAN [29, 41], the trade-off factor is expressed in the form of:

$$\lambda = \frac{2}{\exp(\frac{-10\boldsymbol{epoch}}{\boldsymbol{max\_epoch}})} - 1 \tag{8}$$

where ***epoch*** is the current training epoch, and ***max_epoch*** is the maximum epoch.

In this paper, to enhance the training performance of the model and the transferability of extracted features, we structure a new trade-off factor between classification loss and LMMD loss in following dynamic form:

$$\lambda^* = \frac{-4}{\sqrt{\frac{\boldsymbol{epoch}}{\boldsymbol{max\_epoch}+1}+1}} + 4 \tag{9}$$

To better learn the basic fault feature knowledge, λ^* is set as 0 initially. With the increase of training epoches, for better learning transferable features given the learned fault features of source domain, λ^* starts to increase monotonically, gradually activating the LMMD loss.

In summary, as shown in **Fig. 4**, MDSAN is constructed with the novel shared feature extraction module, subdomain adaptation module based on LMMD and the classifier module. **Algorithm 1** presents the training optimization process of MDSAN.

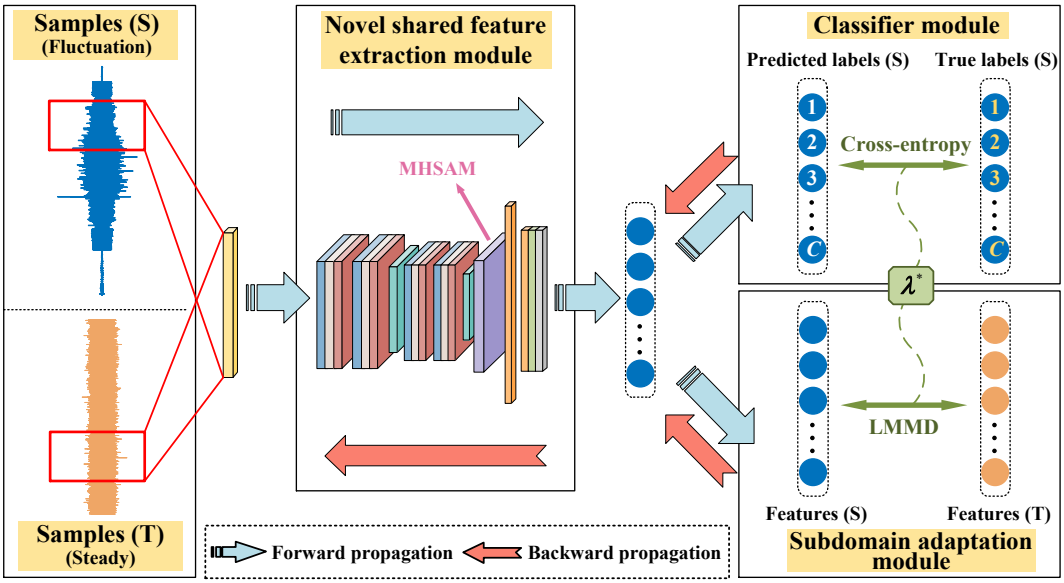

Fig. 4. The framework of the MDSAN

Algorithm 1.Training process of MDSAN

Inputs: Labeled source domain $\mathcal{D}_s$, unlabeled target domain $\mathcal{D}_t$, network architecture, new trade-off factor λ^*, batch size, mini-batch SGD optimizer, ***max_epoch***

Outputs: The trained MDSAN and diagnosis results for target domain samples

Begin: Initialize the training parameter set at random

While not converged **do**

For ***epoch*** =1 **to** ***max_epoch***

For *i*=0,…,*m* **do**

Sample a batch $\{\mathbf{x}_i^s, \mathbf{y}_i^s\}$ from source domain $\mathcal{D}_s$

Sample a batch $\{\mathbf{x}_i^t\}$ from target domain $\mathcal{D}_t$

Extract adaptable features: $\mathbf{z}_i^s$ and $\mathbf{z}_i^t$ by novel shared feature extraction module

Calculate pseudo label of $\mathbf{x}_i^t$: $\hat{\mathbf{y}}_i^t$

Compute $LMMD(\mathbf{z}_i^s, \mathbf{z}_i^t, \mathbf{y}_i^s, \hat{\mathbf{y}}_i^t)$ by **Eq. (6)**

Compute classification loss by the first term **Eq. (7)**

Compute λ^* by **Eq. (9)**

Optimize total loss according to **Eq. (7)**

End for

End for

3.3. The main procedure of the proposed method

The overall procedure can be found in **Fig. 5**, and the main steps can be laconically described as follows.

(1) Acquire vibration acceleration signals of rolling bearings under various operating conditions. Specifically, signals under fluctuating speeds with labels are considered as the source domain and signals under steady speed without labels are considered as the target domain.

(2) Construct the MDSAN model based on a novel shared feature extraction module, a subdomain adaptation module, and a classifier module, in which

(2.1) MHSAM is embedded in the shared feature extraction module to guide to capture the representative features and suppress negative transfer.

(2.2) A new trade-off factor is designed to improve the convergence performance and optimization process for MDSAN.

(3) Input labeled source-domain samples and unlabeled target-domain samples into the constructed MDSAN model for training, and implement fault diagnosis tests.

(4) Compare the proposed method with other popular methods to verify the effectiveness.

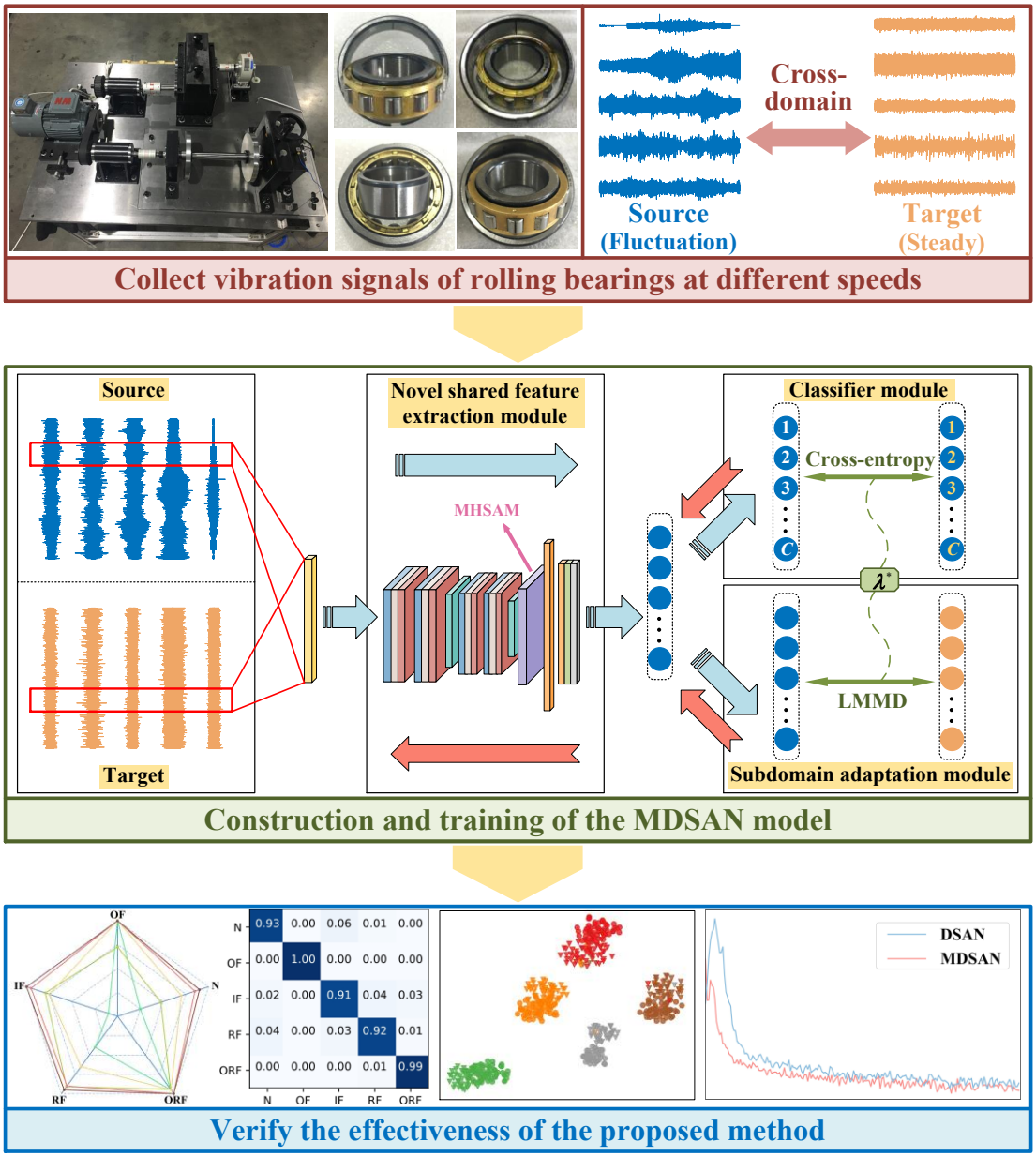

Fig. 5. The overall procedure of the proposed method

4. Case study

4.1. Data description

The bearing test device is given in **Fig. 6**. The rated power of the drive motor is 0.75 kW and the bearing type is QPZZ-II NU205EM cylindrical roller bearing. Fault is indicated by the bearing surface square groove cut by wire cutting technique, with the thresholds: groove width 0.5 mm, depth 0.5 mm wide and 0.5 mm deep. A total of five health conditions of the bearing were simulated: normal (**N**), outer ring fault (**OF**), inner ring fault (**IF**), rolling element fault (**RF**), and outer ring & rolling element compound fault (**ORF**). The faulty bearings are shown in **Fig. 7**. The vibration was mounted at the upper side of the bearing housing. The sample frequency was 25.6 kHz [31].

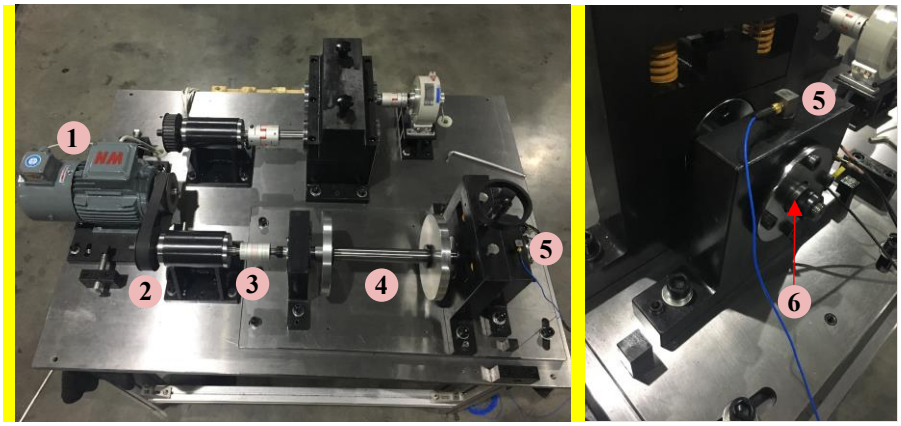

Fig. 6. Test rig of bearing fault diagnosis: ① Controllable speed motor; ② Transmission Belt; ③ Shaft coupling; ④ Rotational shaft; ⑤ Piezoelectric acceleration sensor; ⑥ Tested bearing

(a) **(b)** **(c)** **(d)**

Fig. 7. Photos of four types of faulty bearings: (a) OF; (b) IF; (c) RF; (d) ORF

The source domain data set was collected from the vibration signal with the bearing speed fluctuating irregularly between 800 rpm and 1500 rpm. The target domain data set was collected under the steady speed condition. Five steady speed levels were considered: 1000 rpm, 1100 rpm, 1200 rpm, 1400 rpm, and 1500 rpm. The vibration signals acquired in each of the above conditions are regarded as a separate target domain. A total of 870400 points were collected during the operation of each type of bearing with each health condition under each working condition, and every 1024 points were used as a group as a sample. Hence, 850 samples were divided, i.e., each subdomain contains 850 samples. The vibration signals of five conditions collected in the two domains are shown in **Fig. 8**, and more information about the transfer dataset is shown in **Table 2**.

Table 2

Introduction to the source-domain and target-domain datasets

Domain	Rotational speed	Total sample quantity	Totals of dots per sample
Source domain (S)	Fluctuates irregularly between 800 rpm and 1500 rpm	5×850=4250	1024
Target domain 1 (T1)	1000 rpm (steady)	5×850=4250	1024
Target domain 2 (T2)	1100 rpm (steady)	5×850=4250	1024
Target domain 3 (T3)	1200 rpm (steady)	5×850=4250	1024
Target domain 4 (T4)	1300 rpm (steady)	5×850=4250	1024

Target domain 5 (T5)	1400 rpm (steady)	5×850=4250	1024

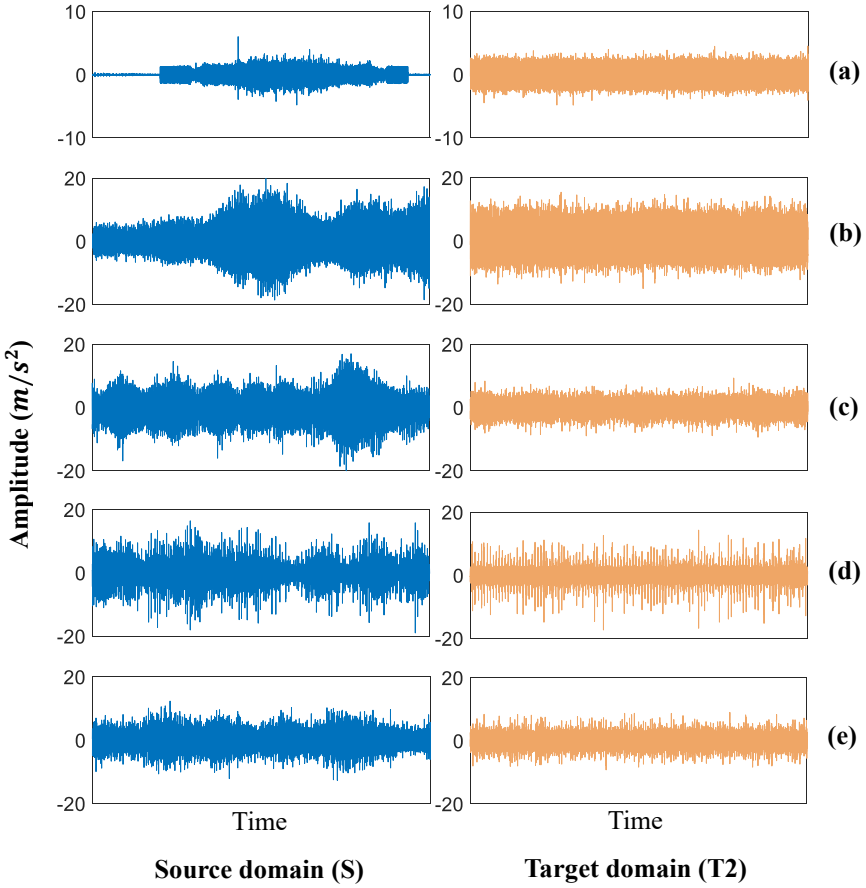

Fig. 8. The original vibrational signals of five bearing health states: (a) N; (b) OF; (c) IF; (d) RF; (e) ORF

4.2. Accuracy comparison with several state-of-the-art methods

To test the capabilities of the proposed method, following state-of-the-art methods are used for comparison: (1) BN-CNN (batch normalization-convolution neural network) [42], (2) AdaBN (adaptive batch normalization) [42-43], (3) MK-MMD (multi kernels maximum mean miscrepancy) [22], (4) JMMD (joint maximum mean discrepancy) [24], (5) DANN (domain adversarial neural network) [23], (6) CDAN (conditional domain adversarial network) [44], and (7) DSAN (deep subdomain adaptation network) [41]. Both MDSAN and comparison methods were tested under pytorch1.12, with batchsize set to 256, max_epoch set to 200, learning rate as 0.001. momentum as 0.9, and weight for adaptation loss as 0.5.

The classified accuracies gained by the above methods are presented in **Table 3** and **Fig. 9**. The proposed method possesses the highest accuracies under all unsupervised cross-domain scenarios containing rotational speed fluctuations, which are 90.08%, 94.50%, 95.97%, 98.73%, and 99.10%, respectively, demonstrating the advantage of MDSAN. The subdomain adaptation strategy endows DSAN and MDSAN with higher classification accuracies than those of the other methods. The accuracy rate given by MDSAN is higher than DSAN in each cross-domain scenario by 1.08%, 2.74%,

2.74%, 1.49%, and 1.30%, respectively, indicating that the MDSAN is more suitable for the speed fluctuation scenario compared to DSAN.

Table 3
Accuracies of different methods under multiple unsupervised cross-domain scenarios

Methods	Unsupervised cross-domain scenarios					Average
	S→T1	S→T2	S→T3	S→T4	S→T5	
BN-CNN	58.86%	71.87%	75.41%	84.18%	77.94%	73.65%
AdaBN	81.81%	85.08%	91.97%	86.68%	96.46%	88.40%
MK-MMD	86.98%	90.23%	93.23%	93.88%	95.57%	91.98%
JMMD	83.72%	86.20%	92.32%	93.36%	95.44%	90.21%
DANN	83.85%	89.19%	92.19%	96.09%	96.48%	91.56%
CDAN	85.55%	88.80%	91.54%	96.22%	97.40%	91.90%
DSAN	89.00%	91.76%	93.23%	97.24%	97.80%	93.81%
MDSAN	**90.08%**	**94.50%**	**95.97%**	**98.73%**	**99.10%**	**95.68%**

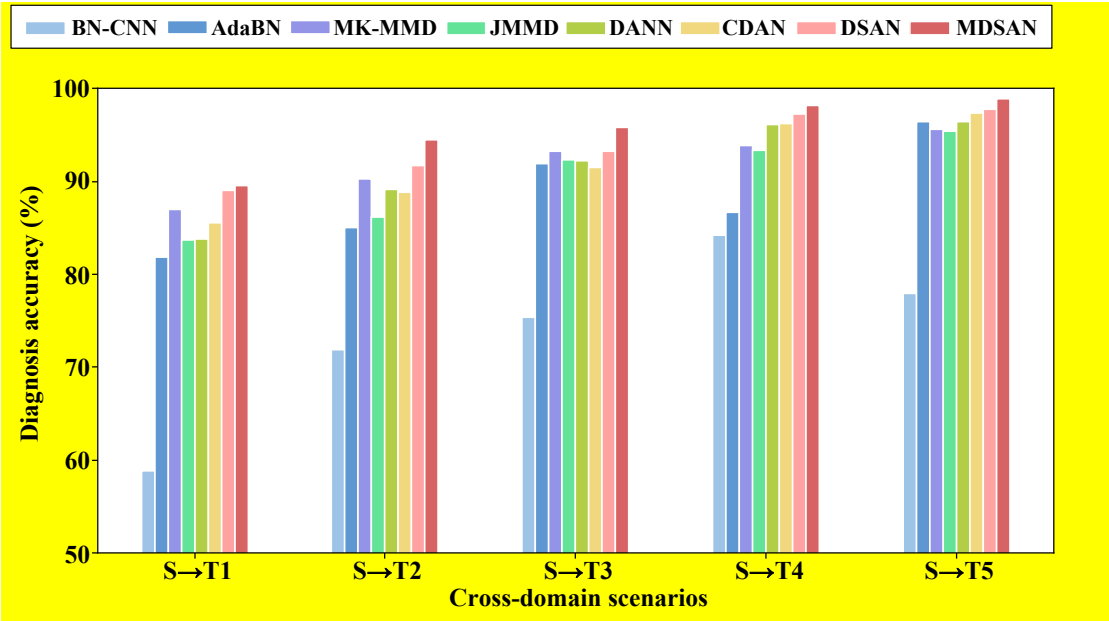

Fig. 9. Accuracies statistics chart of different methods under multiple unsupervised cross-domain scenarios

Fig. 10 shows the accuracies of MDSAN for each class under multiple unsupervised cross-domain scenarios. To have a more straightforward sense of the performance on bearing fault classification under various conditions, taking S→T2 as an example, the 5-classification confusion matrices of the six methods with the highest overall accuracy were drawn in **Fig. 11**, which tells us the proposed approach obtains accuracies higher than 90% in all categories and has good performance on the diagnosis of each class of bearing faults. The proposed approach does not show the phenomenon of

unbalanced diagnostic capability for different classes of faults as exhibited by other methods.

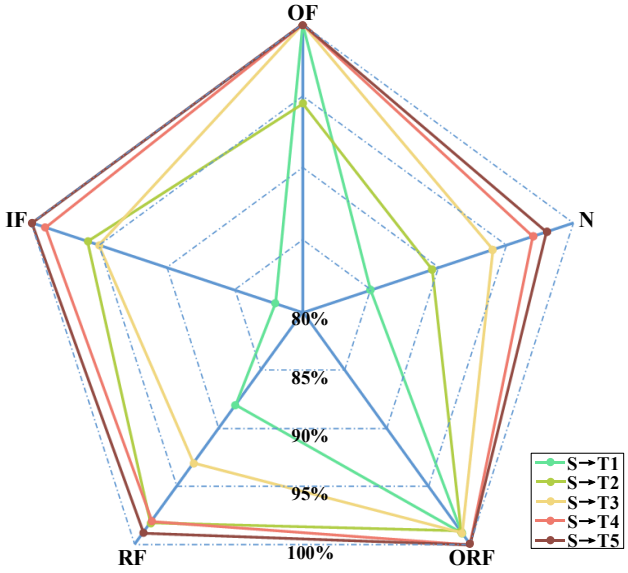

Fig. 10. Diagnosis accuracies of MDSAN for each class under multiple unsupervised cross-domain scenarios

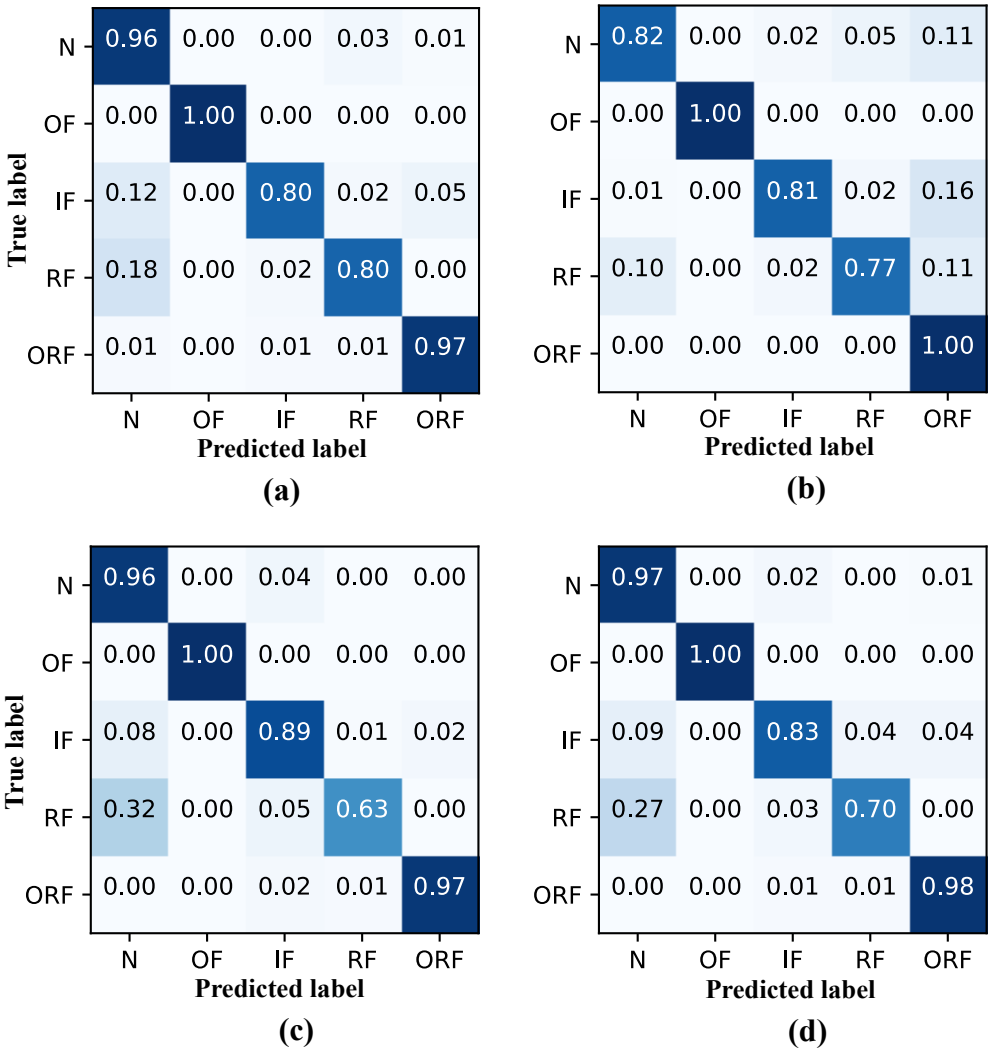

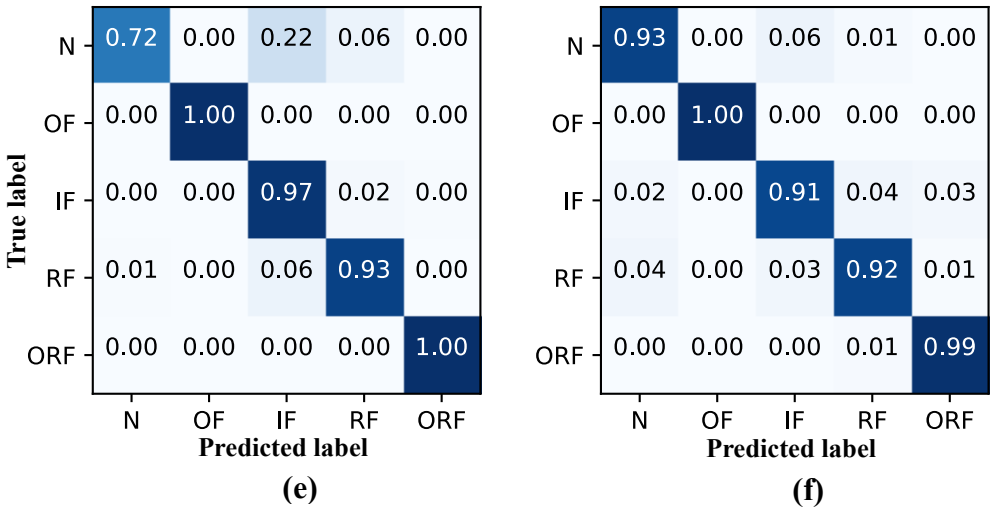

Fig. 11. Confusion matrices of six approaches under unsupervised cross-domain scenario S→T2: (a) MK-MMD; (b) JMMD; (c) DANN; (d) CDAN; (e) DSAN; (f) MDSAN

4.3. Visualization of the extracted features

To compare the transfer behavior of six kinds of methods visually, taking S→T2 for instance, t-distribution Stochastic Neighbor Embedding (t-SNE) [45] is used to visualize the extracted features. The high-dimensional features extracted by the six models are mapped to a two-dimensional plane, as given in **Fig. 12**. It is obvious that DSAN is aligned better than the first four methods because of its strategy of subdomain alignment. However, DSAN have excessive distance between the same class (circled by orange circle in **Fig. 12. (e)**) and non-negligible overlapping areas of subdomains of different classes (circled by blue circle in **Fig. 12. (e)**), which can lead to inaccurate alignment and category confusion. In contrast, MDSAN does not have the above-mentioned drawback. Its feature distribution has smaller distance between the same class (circled by orange circle in **Fig. 12. (f)**) and larger distance between different classes, which is more favorable for transfer learning and fault classification.

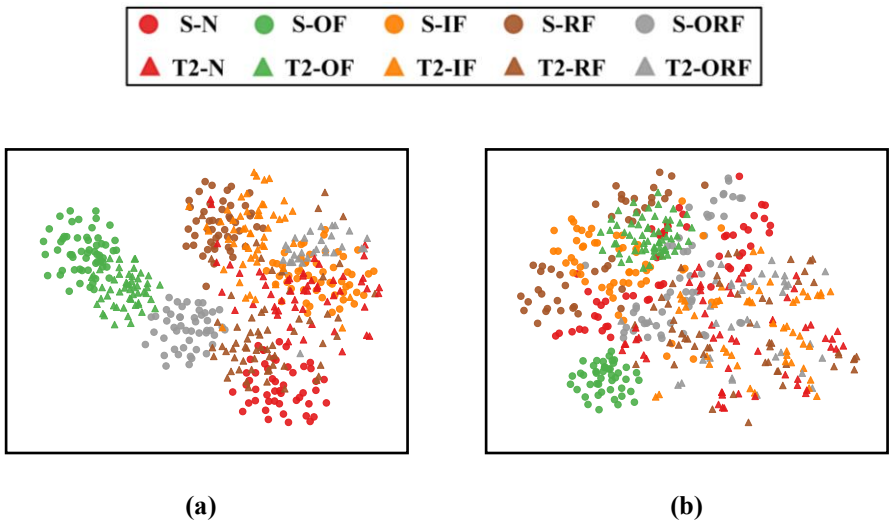

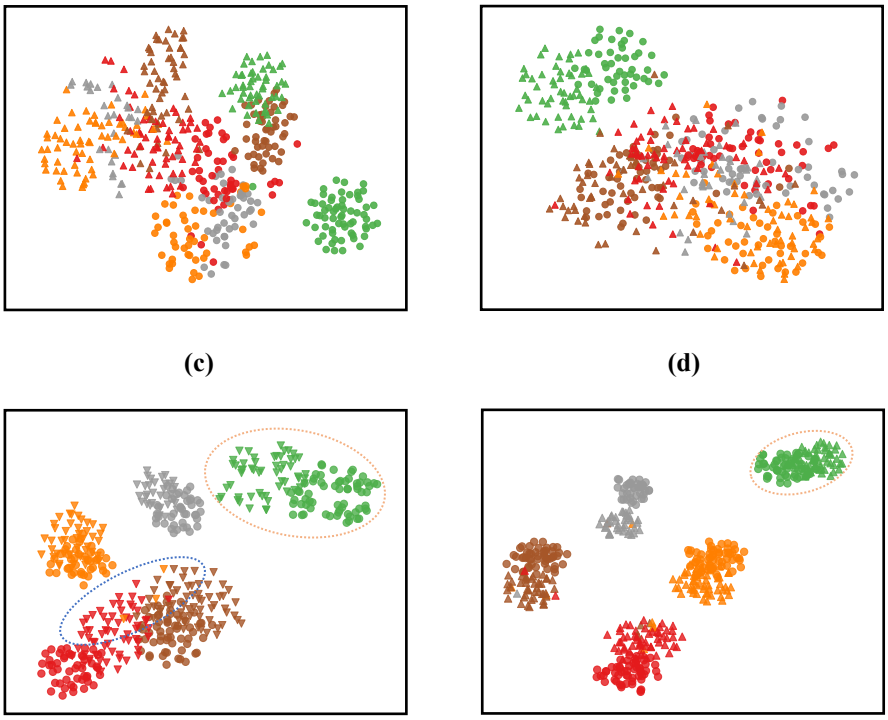

Fig. 12. 2D visualizations of the transferable features: (a) MK-MMD; (b) JMMD; (c) DANN; (d) CDAN; (e) DSAN; (f) MDSAN

4.4. Evolution trends of diagnosis accuracy, LMMD loss and total loss

To further illustrate the performance of MDSAN compared with DSAN, taking S-T2 as an example, the accuracy rate, LMMD loss and total loss of 200 epochs are recorded in turn. As shown in **Fig. 13**, we can find the accuracies of MDSAN rise faster than DSAN, and the LMMD loss and total loss decrease faster, which further illustrates the advanced domain adaptation ability of MDSAN.

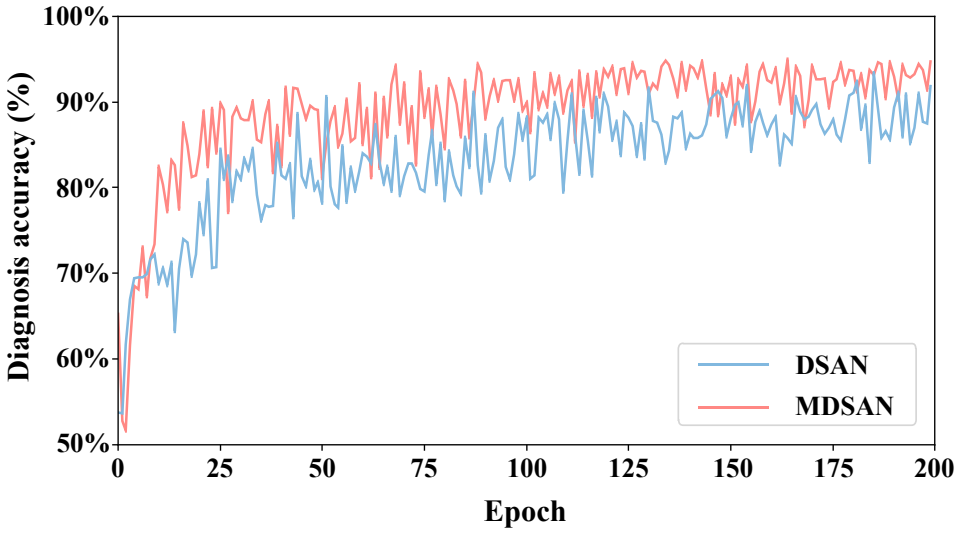

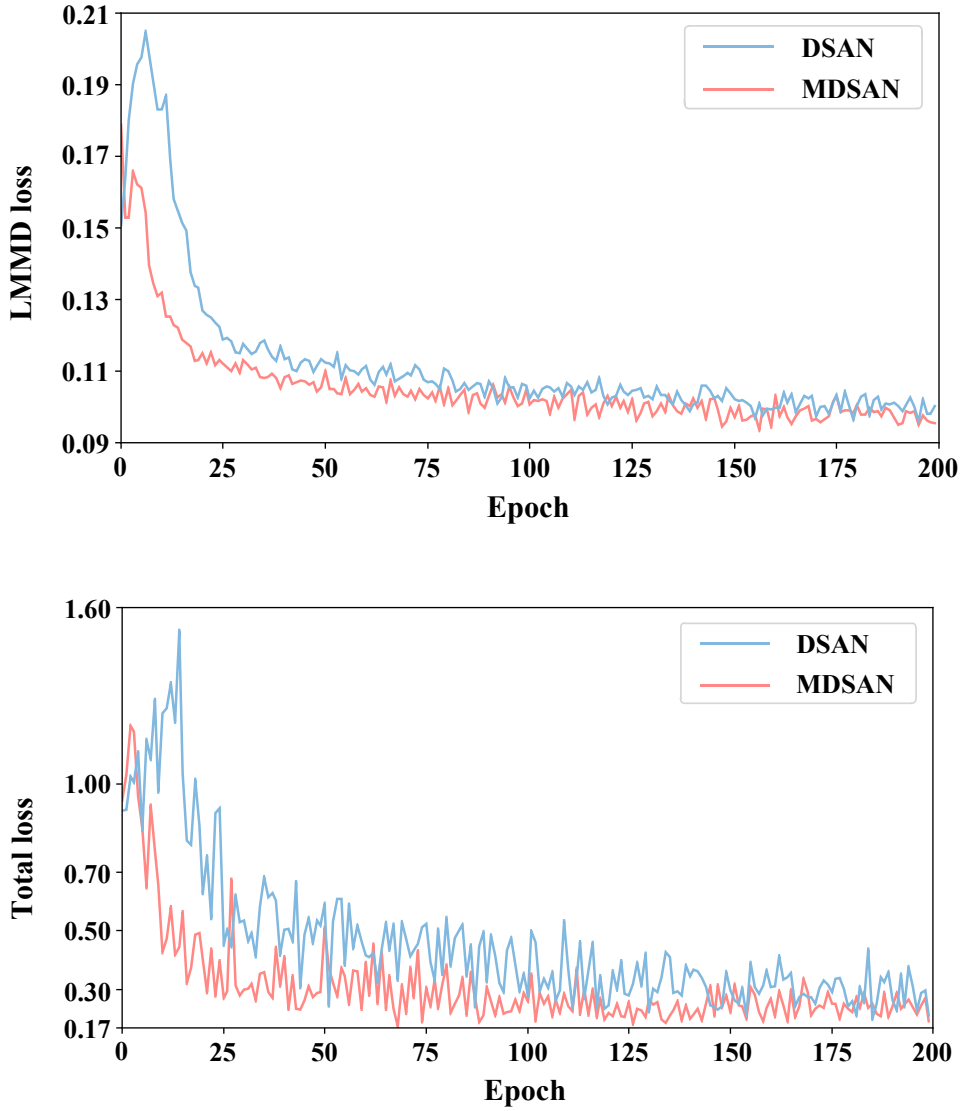

Fig. 13. Evolution trends of diagnosis accuracy, LMMD loss and total loss for DSAN and MDSAN within 200 epochs

5 Conclusions

With the aim of solving problems about unsupervised cross-domain bearing fault diagnosis under speed fluctuation, MDSAN is proposed in this paper, which focuses more on fine features and has stronger feature extraction capability as well as better learning and training capability. In detail, a novel shared feature extraction module guided by multi-headed self-attention mechanism is constructed, and a new trade-off factor is designed for the session of optimizing the objective function.

The presented method was carried out for analyzing the vibrational data of bearings collected under speed fluctuation. The results show that it has higher accuracy, better distribution alignment and faster convergence, in comparison to the existing popular approaches. Subdomain adaptation is a good direction that deserves to be explored in depth. In the future, we will further investigate the topic in the following three aspects. First, when computing the subdomain distribution discrepancy, we can compare the effectiveness of different kernel functions and design a kernel function which is more

suitable for subdomain adaptation. Second, considering inconsistent cross-domain labels in practice, we explore how to use subdomain adaptation methods to implement transfer diagnosis under above scenes. Furthermore, to fully utilize the existing data, we will use multiple source domains containing fluctuating speeds to perform multi-source subdomain adaptation with the unlabeled target domain.

Acknowledgements

This study was supported by the National Natural Science Foundation of China (No. 51905160), the Natural Science Fund for Excellent Young Scholars of Hunan Province (No. 2021JJ20017), and the Student Innovation Training Program (No. S202110532210).

References

[1] He Z, Shao H, Lin J, Cheng J, Yang Y. Transfer fault diagnosis of bearing installed in different machines using enhanced deep auto-encoder. Measurement 2020;152:107393.

[2] Xu Y, Tang X, Feng G, Wang D, Ashworth C, Gu F, Ball A. Orthogonal on-rotor sensing vibrations for condition monitoring of rotating machines. Journal of Dynamics, Monitoring and Diagnostics 2022;1(1):29-36.

[3] Jian C, Ao Y. Industrial fault diagnosis based on diverse variable weighted ensemble learning. Journal of Manufacturing Systems 2022;62:718-35.

[4] Natalia F, Sinha J. Theoretical validation of earlier developed experimental rotor faults diagnosis model. International Journal of Hydromechatronics 2021;4(3):295-308.

[5] Wang W, Lei Y, Yan T, Li N, Nandi A. Residual convolution long short-term memory network for machines remaining useful life prediction and uncertainty quantification. Journal of Dynamics, Monitoring and Diagnostics 2022;1(1):2-8.

[6] He Z, Shao H, Wang P, Lin J, Cheng J, Yang Y. Deep transfer multi-wavelet auto-encoder for intelligent fault diagnosis of gearbox with few target training samples. Knowledge-Based Systems 2020;191:105313.

[7] Wen L, Gao L, Li X, Zeng B. Convolutional neural network with automatic learning rate scheduler for fault classification. IEEE Transactions on Instrumentation and Measurement 2021;70:3509912.

[8] Zhang K, Chen J, He S, Li F, Feng Y, Zhou Z. Triplet metric driven multi-head GNN augmented with decoupling adversarial learning for intelligent fault diagnosis of machines under varying working condition. Journal of Manufacturing Systems 2022;62:1-16.

[9] Deng Y, Du S, Jia S, Zhao C, Xie Z. Prognostic study of ball screws by ensemble data-driven particle filters, Journal of Manufacturing Systems 2020;56:359-72.

[10] Sun J, Gu X, He J, Yang S, Tu Y, Wu C. A Robust Approach of Multi-Sensor Fusion for Fault Diagnosis Using Convolution Neural Network. Journal of Dynamics, Monitoring and Diagnostics 2022:DOI 10.37965/JDMD.2022.95.

[11] Hahn T, Mechefske C. Self-supervised learning for tool wear monitoring with a

disentangled-variational-autoencoder. International Journal of Hydromechatronics 2021: DOI 10.1504/IJHM.2021.114174.

[12] Li W, Huang R, Li J, Liao Y, Chen Z, He G, Yan R, Gryllias K. A perspective survey on deep transfer learning for fault diagnosis in industrial scenarios: Theories, applications and challenges. Mechanical Systems and Signal Processing 2022;167:108487.

[13] Shen C, Wang X, Wang D, Li Y, Zhu J, Gong M. Dynamic joint distribution alignment network for bearing fault diagnosis under variable working conditions. IEEE Transactions on Instrumentation and Measurement 2021;70:3510813.

[14] Zhao B, Zhang X, Zhan Z, Wu Q. Deep multi-scale adversarial network with attention: A novel domain adaptation method for intelligent fault diagnosis. Journal of Manufacturing Systems 2021;59:565-76.

[15] Xiao Y, Shao H, Han S, Huo Z, Wan J. Novel joint transfer network for unsupervised bearing fault diagnosis from simulation domain to experimental domain. IEEE/ASME Transactions on Mechatronics 2022:DOI 10.1109/TMECH.2022.3177174.

[16] Li J, Huang R, He G, Liao Y, Wang Z, Li W. A two-stage transfer adversarial network for intelligent fault diagnosis of rotating machinery with multiple new faults. IEEE/ASME Transactions on Mechatronics 2021;26(3):1591-601.

[17] Deng Y, Du S, Jia S, Zhao C, Xie Z. A double-layer attention based adversarial network for partial transfer learning in machinery fault diagnosis. Computers in Industry 2021;137:103399.

[18] Lin J, Shao H , Min Z, Luo J, Xiao Y, Yan S, Zhou J. Cross-domain fault diagnosis of bearing using improved semi-supervised meta-learning towards interference of out-of-distribution samples. Knowledge-Based Systems 2022;252:109493.

[19] Yang B, Xu S, Lei Y, Lee C, Stewart E, Roberts C. Multi-source transfer learning network to complement knowledge for intelligent diagnosis of machines with unseen faults. Mechanical Systems and Signal Processing 2022;162:108095.

[20] Li J, Zhou K, Qian S, Li W, Duan L, Gao S. Feature Re-Representation and Reliable Pseudo Label Retraining for Cross-Domain Semantic Segmentation. IEEE Transactions on Pattern Analysis and Machine Intelligence 2022:DOI 10.1109/TPAMI.2022.3154933.

[21] Jia S, Deng Y, Lv J, Du S, Xie Z. Joint distribution adaptation with diverse feature aggregation: A new transfer learning framework for bearing diagnosis across different machines. Measurement 2022;187:110332.

[22] Li X, Zhang W, Din Q. A robust intelligent fault diagnosis method for rolling element bearings based on deep distance metric learning. Neurocomputing 2018;310:77-95.

[23] Han T, Liu C, Yang W, Jiang D. A novel adversarial learning framework in deep convolutional neural network for intelligent diagnosis of mechanical faults. Knowledge-Based Systems 2019;165:474-87.

[24] Cao X, Chen B, Zeng N. A deep domain adaption model with multi-task networks for planetary gearbox fault diagnosis. Neurocomputing 2020;409:173-190.

[25] Chen Z, He G, Li J, Liao Y, Gryllias K, Li W. Domain Adversarial Transfer Network for

Cross-Domain Fault Diagnosis of Rotary Machinery. IEEE Transactions on Instrumentation and Measurement 2020;69(11):8702-12.

[26] Qin Y, Yao Q, Wang Y, Mao Y. Parameter sharing adversarial domain adaptation networks for fault transfer diagnosis of planetary gearboxes. Mechanical Systems and Signal Processing 2021;160:107936.

[27] Mao G, Li Y, Jia S, Noman K. Interactive dual adversarial neural network framework: An open-set domain adaptation intelligent fault diagnosis method of rotating machinery. Measurement 2022;195:111125.

[28] Wu Z, Zhang H, Guo J, Ji Y, Pecht M. Imbalanced bearing fault diagnosis under variant working conditions using cost-sensitive deep domain adaptation network. Expert Systems with Applications 2022;193:116459.

[29] Zhu Y, Zhuang F, Wang J, Ke G, Chen J, Bian J, Xiong H, He Q. Deep subdomain adaptation network for image classification. IEEE Transactions on Neural Networks and Learning Systems 2021;32(4):1713-22.

[30] Pan S, Yang Q. A Survey on Transfer Learning. Knowledge and Data Engineering. IEEE Transactions on Knowledge and Data Engineering 2010;22(10):1345-59.

[31] Cao H, Shao H, Zhong X, Deng Q, Yang X, Xuan J. Unsupervised domain-share CNN for machine fault transfer diagnosis from steady speeds to time-varying speeds. Journal of Manufacturing Systems 2022;62:186-98.

[32] Zhou Q, Su Z, Liu L, Hu X, Yu J. Fault diagnosis of rolling bearings based on multi-scale deep subdomain adaptation network. Journal of Intelligent & Fuzzy Systems 2022;43(1):575-85.

[33] Li Y, Wan H, Jiang L. Alignment subdomain-based deep convolutional transfer learning for machinery fault diagnosis under different working conditions. Measurement Science and Technology 2022;33(5):055006.

[34] Tian J, Han D, Li M, Shi P. A multi-source information transfer learning method with subdomain adaptation for cross-domain fault diagnosis. Knowledge-Based Systems 2022;243:108466.

[35] Han S, Shao H, Huo Z, Yang X, Cheng J. End-to-end chiller fault diagnosis using fused attention mechanism and dynamic cross-entropy under imbalanced datasets. Building and Environment 2022;212:108821.

[36] Vaswani A, Shazeer N, Parmar N, Uszkoreit J, Jones L, Gomez A, Kaiser L, Polosukhin I. Attention Is All You Need. 31st Annual Conference on Neural Information Processing Systems (NIPS). Long Beach, CA. 2017:1-15.

[37] Han Z, Shang M, Liu Z, Vong C, Liu Y, Zwicker M, Han J, Chen C. SeqViews2SeqLabels: Learning 3D Global Features via Aggregating Sequential Views by RNN With Attention. IEEE Transactions on Image Processing 2019;28(2):658-72.

[38] Ioffe S, Szegedy C. Batch normalization: Accelerating deep network training by reducing internal covariate shift. 32nd International Conference on Machine Learning. Lille, FRANCE. 2015;37:448-56.

[39] Gretton A, Borgwardt K, Rasch M, Scholkopf B, Smola A. A kernel two-sample test. Journal of Machine Learning Research 2012;13:723-73.

[40] Mohsenzadeh Y, Sheikhzadeh H. Gaussian Kernel Width Optimization for Sparse Bayesian Learning. IEEE Transactions on Neural Networks and Learning Systems 2015;24(4):709-19.

[41] Ghorvei M, Kavianpour M, Beheshti, M, Ramezani A. An Unsupervised Bearing Fault Diagnosis Based on Deep Subdomain Adaptation Under Noise and Variable Load Condition. Measurement Science and Technology 2022;33(2):025901.

[42] Zhao Z, Zhang Q, Yu X, Sun C, Wang S, Yan R, Chen X. Applications of Unsupervised Deep Transfer Learning to Intelligent Fault Diagnosis: A Survey and Comparative Study. IEEE Transactions on Instrumentation and Measurement 2021;70:3525828.

[43] Li Y, Wang N, Shi J, Hou X, Liu J. Adaptive batch normalization for practical domain adaptation. Pattern Recognition 2018;80:109-17.

[44] Long M, Cao Z, Wang J, Joedan M. Conditional adversarial domain adaptation. 32nd Conference on Neural Information Processing Systems (NIPS). Montreal, CANADA. 2018;31:1647-57.

[45] Laurens V D M, Hinton G. Visualizing data using t-SNE. Journal of Machine Learing Research 2008;9(2605):2579-605.